Shake table experiment on RC bridge columns using E-Defense

by

Kazuhiko Kawashima[1], Tomohiro Sasaki[2], Koichi Kajiwara[3], Hiromichi Ukon[4], Shigeki Unjoh[5], Junichi Sakai[6], Kenji Kosa[7], Yoshikazu Takahashi[8], Masaaki Yabe[9] and Hiroshi Matsuzaki[10]

ABSTRACT

This paper presents preliminary results of a large scale shake table experiment conducted to study the failure mechanism of reinforced concrete bridge columns. E-Defense which was constructed by National Institute for Earth Science and Disaster Prevention was used to excite three columns; a typical flexural failure dominant column in the 1970s (C1-1 column), a typical shear failure dominant column in the 1970s (C1-2 column) and a typical column designed in accordance with the current design code (C1-5 column). They were 7.5 m tall 1.8-2.0 m diameter circular reinforced concrete columns. They were subjected to a near-filed ground motion recorded during the 1995 Kobe, Japan earthquake. Preliminary results on the experiment and analytical correlation are presented.

1. INTRODUCTION

Bridges are a vital component of transportation facilities; however it is known that bridges are vulnerable to the seismic effect. Bridges suffered extensive damage in past earthquakes such as 1989 Loma Prieta earthquake, 1994 Northridge earthquake, 1995 Kobe earthquake, 1999 Chi Chi earthquake, 1999 Bolu earthquake and 2008 Wenchuan earthquake. A large scale bridge experimental program was initiated in 2005 in the National Research Institute for Earth Science and Disaster Prevention (NIED), Japan as one of the three US-Japan cooperative research programs based on NEES and E-Defense collaboration. In the bridge program, it was originally proposed to conduct experiments on two model types; 1) component models and 2) system models. They are called hereinafter as C1 experiment and C2 experiment, respectively [1].

The objective of the C1 experiment is to clarify the failure mechanism of reinforced concrete columns using models with as large section as possible. On the other hand, C2 experiment was proposed to clarify the system failure mechanism of a bridge consisting of decks, columns, abutments, bearings, expansion joints and unseating prevention devices.

C1 experiment was conducted for two typical reinforced concrete columns which failed during the 1995 Kobe earthquake (C1-1 and C1-2 experiments) and a typical reinforced concrete column designed in accordance with the current design requirements (C1-5 experiment). This paper shows preliminary results of the experiment and analysis on three C1 columns.

2. EXPERIMENTAL SETUP AND COLUMN MODELS

Photo 1 shows the experimental setup of three columns using E-Defense [2]. Two simply supported decks were set on the column and on the two steel end supports. A catch frame was set

1 Professor, Department of Civil Engineering, Tokyo Institute of Technology, Meguro, Tokyo, Japan
2 Graduate student, ditto
3 Senior researcher, Hyogo Earthquake Engineering Research Center, National Research Institute for Earth Science and Disaster Prevention, Miki, Hyogo, Japan
4 Research Fellow, ditto
5 Chief Researcher, Center for Advanced Engineering Structural Assessment and Research, Public Works Research Institute, Tsukuba, Japan
6 Senior Researcher, ditto
7 Professor, Department of Civil Engineering, Kyushu Institute of Technology, Kita Kyushu, Japan
8 Associate Professor, Disaster Prevention Research Institute, Kyoto University, Uji, Japan
9 General Manager, Earthquake Engineering Division, Chodai, Tsukuba Science City, Japan
10 Assistant Professor, Department of Civil Engineering, Tokyo Institute of Technology, ditto

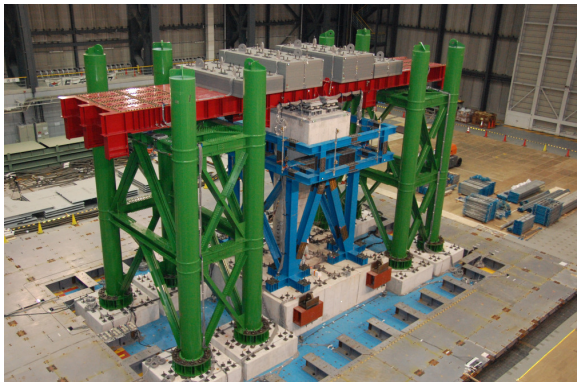

Photo 1 C1 on E-Defense

under the lateral beam of the column to prevent collapse of the column when it was excessively damaged. Tributary mass to the column by two decks including four weights was 307 t and 215 t in the longitudinal and transverse directions, respectively. The tributary mass was increased by 21 % from 307 t to 372 t in a part of C1-5 excitation.

Three full-size reinforced concrete columns as shown in Fig. 1 were constructed for the experiment. Columns used for C1-1, C1-2 and C1-5 experiments, which are called hereinafter as C1-1, C1-2 and C1-5, respectively, are 7.5 m tall reinforced concrete columns with a diameter of 1.8 m in C1-1 and C1-2 and 2 m in C1-5. C1-1 and C1-2 are typical columns which were built in the 1970s based on a combination of the static lateral force method and the working stress design in accordance with the 1964 Design Specifications of Steel Road Bridges, Japan Road Association. Since it was a common practice prior to 1980 to terminate longitudinal bars at mid-heights, the inner and center longitudinal bars were cut off at 1.86 m and 3.86 m from the column base, respectively. The cut-off heights were determined by extending a length equivalent to a lap splicing length l_{ls} (about 30 times bar diameter) from the height where longitudinal bars became unnecessary based on the moment distribution. On the other hand, longitudinal bars were not cut-off in C1-1. C1-1 and C1-2 had the same shape, heights, bar arrangement and properties except the cut-off. As a consequence, C1-1 failed in flexure while C1-2 failed in shear, as will be described later. The shear failure due to cut-off was one of

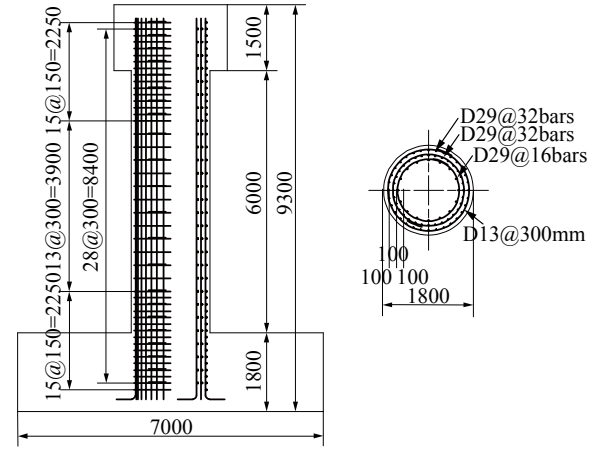

(a) C1-1

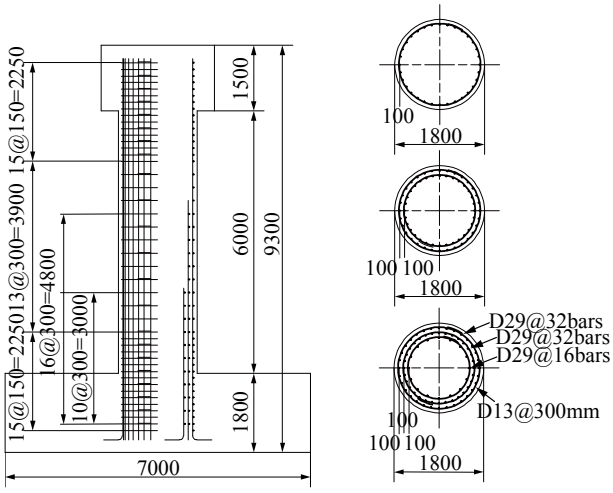

(b) C1-2

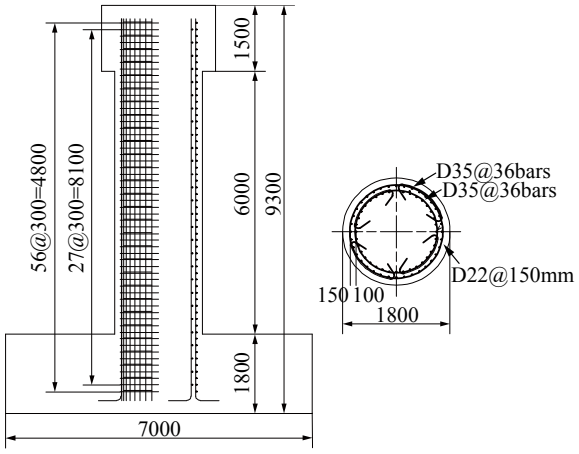

(c) C1-5

Fig. 1 C1 column models

the major sources of the extensive damage of bridges in the 1995 Kobe earthquake [3].

Table 1 Seismic performance of C1-1 and C1-5 in longitudinal direction based on 2002 JRA code

Demand and Capacity	Model Columns	C1-1	C1-5(1)	C1-5(2) and C1-5(3)
Lateral Force	Design response acceleration S_A (m/s²)	1.75 × 9.8 m/s² = 17.16		
	Force reduction factor $R = \sqrt{2\mu_d - 1}$	1.58	2.56	2.54
	Acceleration demand S_A / R (m/s²)	10.83	6.70	6.77
Demand	Lateral force (kN)	3,271	2,023	2,824
	Lateral displacement u (m) ($\mu = u / u_y$)	0.328	0.168	0.183
Capacity	Lateral force P_u (kN)	1,614	2,341	2,371
	Yield displacement u_y (m)	0.046	0.045	0.045
	Design displacement u_d (m) ($\mu_d = u_d / u_y$)	0.081	0.169	0.166
	Ultimate displacement u_u (m) ($\mu_u = u_u / u_y$)	0.099	0.231	0.227

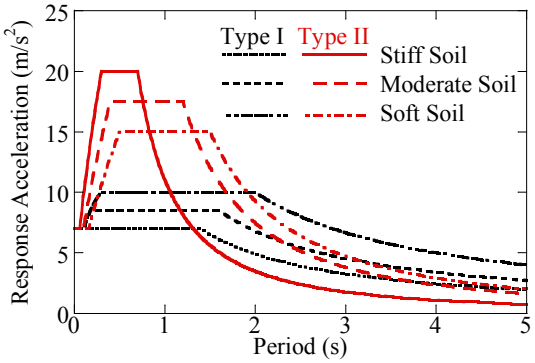

Fig. 2 Design response spectra (2002 JRA)

Combination of the lateral seismic coefficient of 0.23 and the vertical seismic coefficient of +/-0.11 (upward and downward seismic force) was assumed in the design of C1-1 and C1-2.

Deformed 13 mm diameter circular ties were provided at 300 mm interval, except the outer ties at the top 1.15m zone and the base 0.95 m zone where they were provided at 150mm interval in C1-1. Ties were only lap spliced with 30 times the bar diameter. Lap splice was a common practice by the mid 1980s. The longitudinal and tie bars had a nominal strength of 345 MPa (SD345), and the design concrete strength was 27 MPa. The longitudinal reinforcement ratio P_l was 2.02 % and the volumetric tie reinforcement ratio ρ_s was 0.32 % except the top 1.15 m and base 0.95m zones where ρ_s was 0.42% in C1-1. P_l and ρ_s varied depending on the zones in C1-2; 2.02 % and 0.42 % at the base 0.95 m zone, 2.02 % and 0.32 % between 0.95 m and 1.86 m, 1.62 % and 0.21 % between 1.86 m and 3.86 m, 0.81 % and 0.11 % between 3.86 m and 4.85 m, and 0.81 % and 0.21 % at the top 1.15 m zone, respectively.

On the other hand C1-5 was designed in accordance with the 2002 JRA Design Specifications of Highway Bridges (JRA 2002) based on the design response spectrum as shown in Fig. 2. Sixty four deformed 35mm diameter longitudinal bars were provided in two layers. Deformed 22 mm diameter circular ties were set at 150 mm and 300 mm interval in the outer and inner longitudinal bars, respectively. The ties were developed in the core concrete using 135 degree bent hooks after lap spliced with 40 times the bar diameter. The nominal strength of longitudinal and tie bars and the design concrete strength were the same with those in C1-1 and C1-2 columns. The longitudinal reinforcement ratio P_l was 2.19 % and the volumetric tie reinforcement ratio ρ_s was 0.92 %

Table 1 shows the evaluation of the seismic performance of C1-1 and C1-5 in the longitudinal direction based on the 2002 JRA code. Because

the design response acceleration S_A is 17.15 m/s^2 for both C1-1 and C1-5, the yield displacement u_y and ultimate displacement u_u are 0.046 m and 0.099 m in C1-1 and 0.045 m and 0.231 m in C1-5. The design displacement u_d is evaluated from u_y and u_u as

$$u_d = u_y + \frac{u_u - u_y}{\alpha} \quad (1)$$

in which α depends on the type of ground motion (near-field or middle field ground motion) and the importance of the bridge. Assuming α is 1.5 for a combination of the near-field ground motion category and the important bridges category, the design displacement u_d is 0.081 m in C1-1 and 0.169 m in C1-5.

On the other hand, the displacement demand u is 0.328 m in C1-1 and 0.168 m in C1-5 because the force reduction factor is 1.58 and 2.56 respectively. Consequently, C1-1 and C1-5 were evaluated to be unsafe and safe, respectively based on the current design code.

Three columns were excited using a near-field ground motion as shown in Fig. 3 which was recorded at the JR Takatori Station during the 1995 Kobe earthquake. It was one of the most influential ground motions to structures. However duration was short. Taking account of the soil structure interaction, a ground motion with 80% the original intensity of JR Takatori record was imposed as a command to the table in the experiment. This ground motion is called hereinafter as the 100 % E-Takatori ground motion. Excitation was repeated to clarify the seismic performance of the columns when they were subjected to near-field ground motions with longer duration and/or stronger intensity. Only C1-5 was excited using 125 % E-Takatori ground motion with 21 % increased deck mass to study the seismic performance under a stronger ground motion than the JR-Takatori Station ground motion.

3. SEISMIC PERFORMANCE OF C1-1 AND C1-5

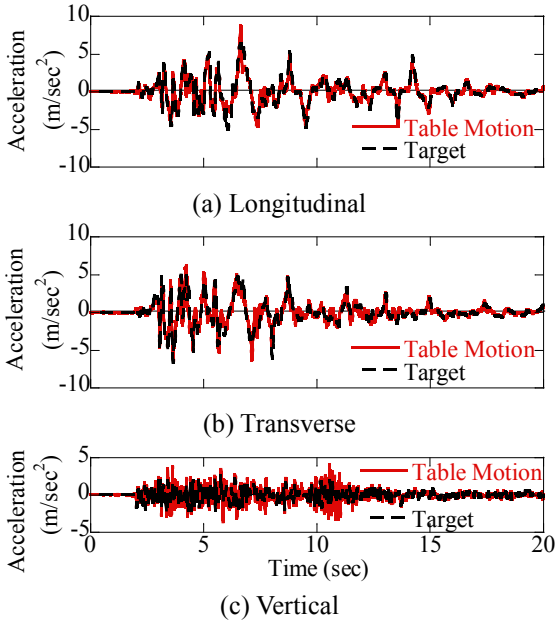

Fig. 3 100% E-Takatori ground motion (C1-5(1)-1 excitation)

3.1 Progress of Failure

C1-1 was subjected to the 100 % E-Takatori ground motion twice. Photo 2 shows the progress of failure at the plastic hinge on the SW surface where damage was most extensive. NS and EW direction correspond to the transverse and longitudinal directions, respectively, of the model. During the first excitation (C1-1-1 excitation), at least two outer longitudinal bars from S to W locally buckled between the ties at 200 mm and 500 mm from the base. During the second excitation (C1-1-2 excitation), both the covering and core concrete suffered extensive damage between the base and 0.7 m from the base on the SW surface. Three ties from the base completely separated at the lap splices. Eleven outer and three center longitudinal bars locally buckled between ties at 50 mm and 500 mm from the base.

On the other hand, C1-5 was subjected to the 100% E-Takatori ground motion twice (C1-5(1)-1 and C1-5(1)-2 excitations). After the mass was increased by 21 % from 307 t to 372 t, C1-5 was subjected to the 100% E-Takatori ground motion once (C1-5(2) excitation). Then C1-5 was subjected to the 125% E-Takatori ground motion twice (C1-5(3)-1 and C1-5(3)-2 excitations).

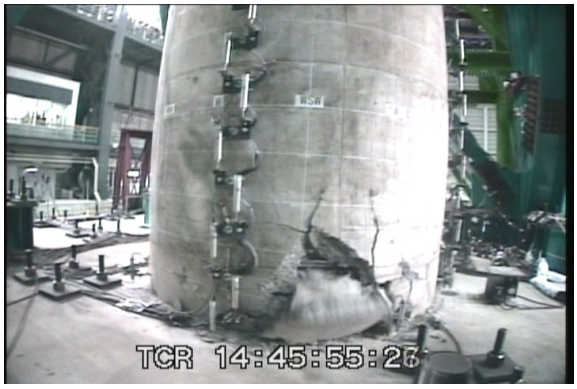

(a) C1-1-1 excitation (8.35s)

(a) C1-5(2) excitation (8.80s)

(b) C1-1-2 excitation (7.71s)

Photo 2 Progress of damage of C1-1

(b) C1-5(3)-2 excitation (7.17s)

Photo 3 Progress of damage of C1-5

Photo 3 shows the progress of failure of C1-5 at the plastic hinge during C1-5(1)-1, C1-5(2) and C1-5(3)-2 excitations. During C1-5(1)-1 excitation, only a few flexural cracks with the maximum width of 1mm occurred around the column at the plastic hinge. Therefore it is noted that the seismic performance is enhanced in C1-5 than C1-1 under the first 100% E-Takatori excitation. The damage progressed during C1-5(2) excitation such that the covering concrete spalled off at the 500 mm base zone from WSW to SSW. During C1-5(3)-2 excitation, the failure extensively progressed. The core concrete crashed due to repeated compression, and blocks of crashed core concrete spilled out from the steel cages like explosion. Such a failure was never seen in the past quasi-static cyclic or hybrid loading experiments. Because the maximum aggregate size was 20 mm, the concrete blocks after crashed can be as small as 20-40 mm. Because the gaps of longitudinal bars and circular ties were 132mm and 128mm, respectively, it was possible for the blocks of crashed core concrete to move out from the steel cages. Furthermore twelve outer longitudinal bars and nineteen inner longitudinal bars locally buckled on SW and NE-E surfaces. The 135 degree bent hooks developed in the core concrete still existed in the original position although the core concrete around the hooks suffered extensive damage.

3.2 Response Displacement and Moment Capacity

Figs. 4 and 5 show the response displacement at the top of C1-1 and C1-5, respectively, in the principal response direction (nearly SW-NE direction). The peak displacement of C1-1 was 0.179 m (2.4 % drift) during C1-1-1 excitation while the peak displacement of C1-5 was 0.084 m (1.1 % drift) during C1-5(1)-1 excitation. Because the ultimate displacement in accordance with JRA 2002 code was 0.100 m and 0.235 m in C1-1 and C1-5, respectively, the above peak response

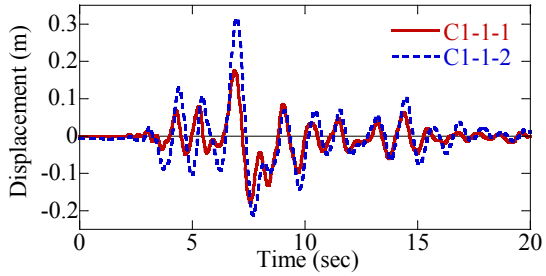

Fig. 4 Response displacement at the top of C1-1 in the principle response direction

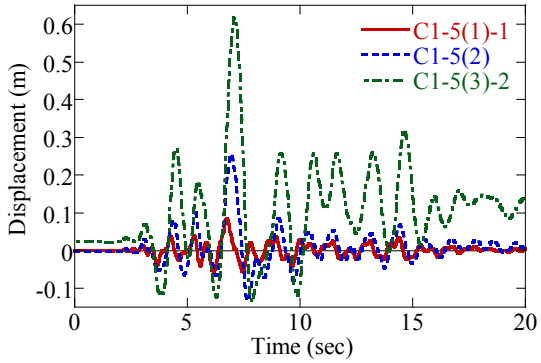

Fig. 5 Response displacement at the top of C1-5 in the principle response direction

displacements corresponded to 179 % and 36 % the ultimate displacement in C1-1 and C1-5, respectively.

Figs. 6 and 7 show the moment at the column base vs. lateral displacement at the column top hystereses of C1-1 and C1-5, respectively, in the principal response direction. The computed moment vs. lateral displacement relations based on the 2002 JRA code are also shown here for comparison. The moment capacity of C1-1 during C1-1-2 excitation was 13.41 MNm which deteriorated by 19 % from the moment capacity during C1-1-1 excitation of 16.47 MNm. On the other hand, the moment capacity of C1-5 column progressed from 19.82 MNm during C1-5(1)-1 excitation to 20.14 MNm and 24.85 MNm during the C1-5(2) and C1-5(3)-2 excitations, respectively. However since the moment capacity of C1-5 during the C1-5(3)-1 excitation was 25.54 MNm, the moment capacity of C1-5 deteriorated by 3% during C1-5(3)-2 excitation. The computed moment capacities are close to the experimental values in both C1-1 and C1-5, however the

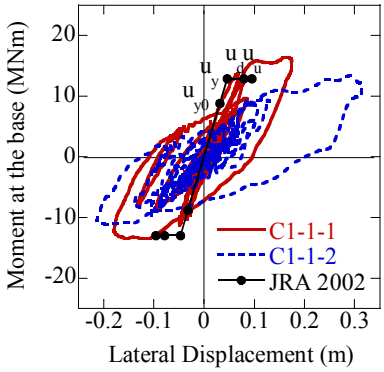

Fig. 6 Moment at the base vs. lateral displacement at the column top hysteresis of C1-1 in the principle response direction

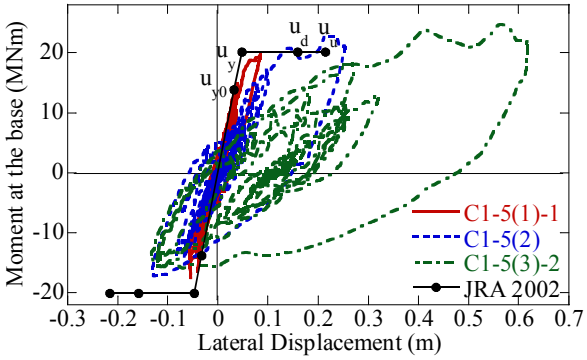

Fig. 7 Moment at the base vs. lateral displacement at the column top hysteresis of C1-5 in the principle response direction

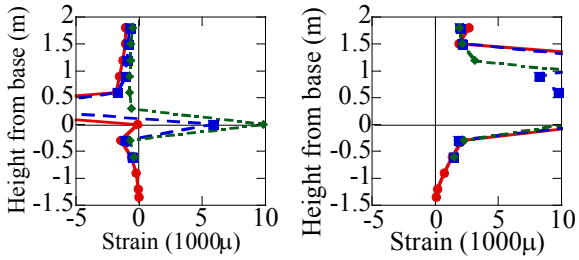

(a) W surface (b) E surface

Fig. 8 Stains of longitudinal reinforcements at 6.9 s during C1-1-1 excitation

computed ultimate displacement are very conservative compared to the experiment.

3.3 Deformation of Longitudinal Bars

Fig. 8 shows the strain distribution of the longitudinal bars in the vertical direction in C1-1 during C1-1-1 excitation at 6.9s when the response displacement in the principal response

direction took a peak value. Strains in the longitudinal bars were over 10,000 μ in tension at the SE, E, NE, N and NW surfaces while they were over 5,000 μ in compression at the SW and W surfaces. The fact that large compression strains developed in the longitudinal bars implies that the core concrete had already been damaged allowing local buckling of longitudinal bars to occur. Strains in the longitudinal bars are extremely large between 0.25 m below and 1.5 m above the base of the column. Because the plastic hinge length is a half width of the column (0.9 m) based on the design code, it is important to note that longitudinal bars extensively yielded at the zone above the plastic hinge region.

3.4 Deformation of Circular Ties

Fig. 9 shows the strains of circular ties in C1-1 at 6.9 s during C1-1-1 excitation. In particular, strain distribution along ties at 350 mm and 650 mm from the base are shown. Strains of tie bars reached nearly 2,000 μ, slightly larger than the yield strain. Consequently the ties were still in the elastic or slightly inelastic range. It is important to note that strains in the outer ties are larger along the SW and W surfaces where the section is subjected to compression. As will be described later, this resulted from the local buckling of longitudinal bars at the SW surface.

It should be noted in Fig. 9 that the lateral confinement by ties is very complex. The lateral confinement is not uniform around the ties as it is generally assumed when the lateral confinement is evaluated in design (JRA 2002). The tie strains are not the same among the three ties. For example, outer bars yielded at the SW and W surfaces while strains of center and inner ties are still less than 1,000 μ at 350 mm.

Fig. 10 shows strains of three ties at 350 mm from the base vary at 6.9 s and 7.6 s in C1-1. Strains are generally larger in the outer ties than the center and inner ties. It is noted that strain of a tie in a layer (outer, center or inner) becomes large independently with ties in other layers. For example, strain of an outer tie at 7.6 s is largest at NE (1,513 μ), but strains of center and inner ties are small. On the other hand, strain of an inner tie

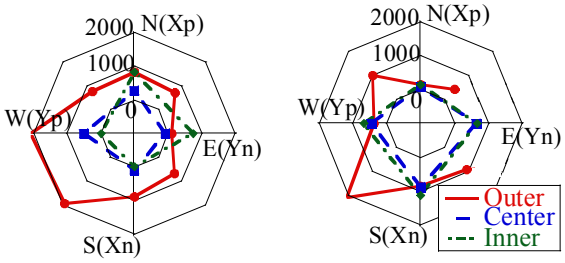

(a) 350 mm from base (b) 650 mm from base

Fig. 9 Strains of ties at 6.9 s during C1-1-1 excitation

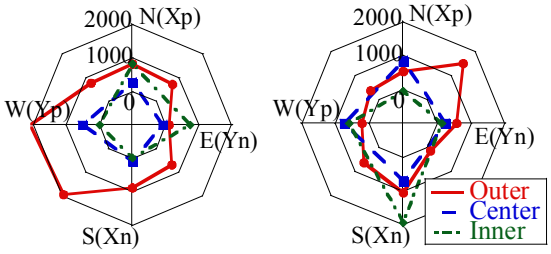

(a) 6.9 s (b) 7.6 s

Fig. 10 Strains of Ties at 350 mm from base

at 7.6s is largest at S (1,925 μ) but strains of center and outer ties are small. Based on the current design code, the volumetric tie reinforcement ratio ρ_s is evaluated as

$$\rho_s = \rho_{sO} + \rho_{sC} + \rho_{sI} \qquad (2)$$

where, ρ_{sO}, ρ_{sC} and ρ_{sI} are volumetric tie reinforcement ratio of the outer, center and inner ties, respectively. However Fig. 10 shows that estimation of the volumetric tie reinforcement ratio by Eq. (2) can be overestimated. Mechanism of the lateral confinement by multi-layered tiesshould be critically clarified.

Fig. 11 shows the strains in the outer, center and inner layers of both longitudinal bars and tie bars. Because a compression strain over 15,000 μ developed in the outer longitudinal bar at 6.9 s, buckling of the outer longitudinal bar must have occurred at this time. It is important to note that strain of the outer tie reached 2,300 μ at the same time. This implies a mechanism that the outer tie restricted the local buckling of the outer longitudinal bar, and that this resulted in a sharp

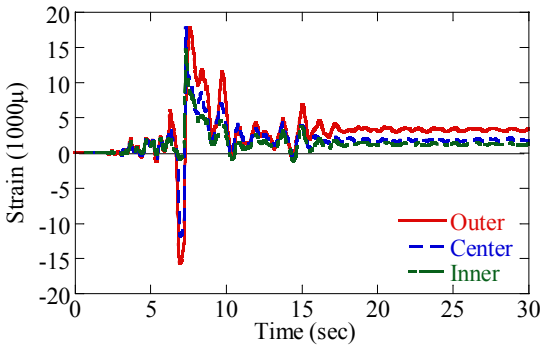

(a) Longitudinal bars

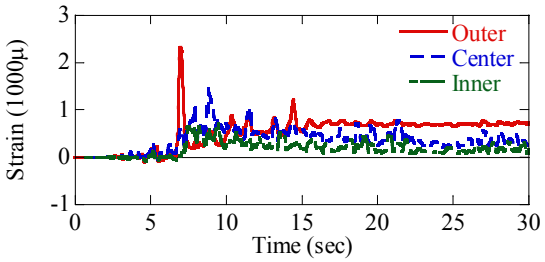

(b) Tie bars

Fig. 11 Strains of longitudinal bars at 300 mm and tie bars at 350 mm from base at W surface

increase of strain in the outer tie.

Fig. 12 shows the interaction of a longitudinal bar 300 mm from the base and a tie bar 350 mm from the base at the W surface. Fig. 12 (a) shows the hysteresis of strains of the outer longitudinal bar and the outer tie. An increase of strain in the outer tie which resulted from restraining the local buckling of the outer longitudinal bar under high compression strain is clearly seen. On the other hand, such an increase of strain in the outer tie is not seen in the center and inner bars as shown in Fig. 12 (b) and (c) because longitudinal bars did not yet buckle.

4. SEISMIC PERFORMANCE OF C1-2

4.1 Progress of Failure

Photo 4 shows the progress of failure of C1-2 on NW and SE surfaces. A horizontal crack first developed at 4.10s along NW to E surface, and it progressed to a shear crack at 4.33 s. Another horizontal crack developed at 4.60s along W to SE surface, and it extended to at least two diagonal cracks at 4.87s. Among two diagonal cracks

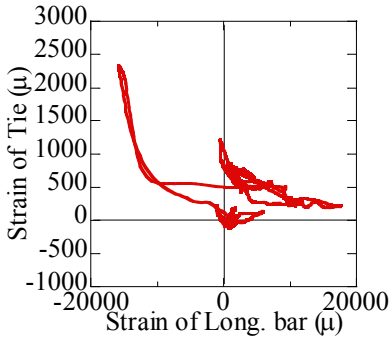

(a) Outer layer

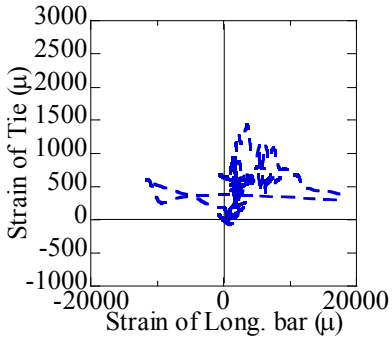

(b) Center layer

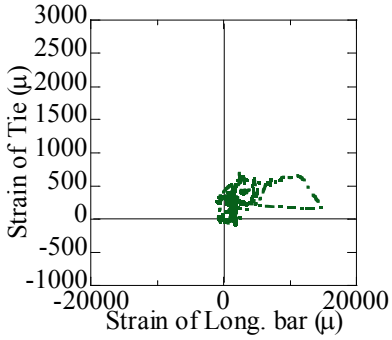

(c) Inner layer

Fig. 12 Longitudinal bar dtrain at 300 mm vs. tie bar strain at 350 mm from base at W surface

developed at 4.33 s, a crack on NW surface extended to W surface, and the other crack on SE surface extended to S at 5.37s. The core concrete started to crash due to shear, and the blocks of crashed core concrete started to move out from the inside of the column near the upper cut-off on N and NW surfaces at 6.04 s. The same but more extensive failure occurred on S and SW surfaces at 6.50 s. The blocks of crashed core concrete progressively moved out from steel cages associated with the column response in the SW

(a) NW

(b) SE

(1) 6.50s

(a) NW

(b) SE

(2) 6.87s

Photo 4 Progress of damage of C1-2

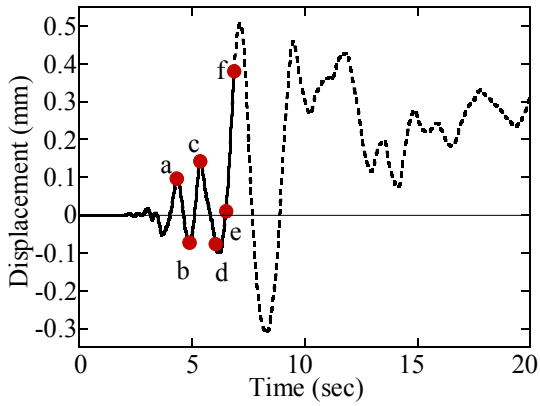

Fig. 13 Response displacement of C1-2 in the principal response direction

direction.

At 6.87 s, the bottom of lateral beam hit with the upper surface of catch frame due to excessive response displacement. Three circular tie bars completely separated at their lap splice and the longitudinal bars deformed in the outward direction. Extensive failure of core concrete and deformation of longitudinal bars progressed on W, NW, N, NE and E surfaces.

It should be noted in the above process that the failure of core concrete was extensive and a large numbers of blocks of crashed core concrete as well as deformed longitudinal bars moved out from inside of the column during very short time (less than 3 s). It was like an explosion.

4.2 Response and Shear Capacity

Fig. 13 shows response displacement of C1-2 in the principal response direction. As described above, since bottom of the lateral beam hit with the upper surface of catch frame at 6.87 s, the column response after 6.87 s was affected by this contact. Without the catch frame, the column possibly overturned. Therefore the response displacement after this contact is plotted by dotted line in Fig. 13. At 7.125 s, right after the contact, the column response displacement reached its peak of 439.2 mm and 253.0 mm in the longitudinal and transverse directions, respectively. Residual drifts of 204.5 mm and 343.2 mm were developed after the excitation.

Fig. 14 shows the lateral force at the upper cut-off vs. lateral displacement at the column top hysteresis in the principal response direction. The hysteresis after the contact of the column with the catch frame is plotted by dotted line. The shear capacity of the column F_s was evaluated based on the truss theory as [4]

$$F_s = F_{sc} + F_{ss} \tag{3}$$

where

$$F_{sc} = c_c \tau_c b d \tag{4}$$

$$F_{ss} = \frac{A_h \sigma_{sy} d}{1.15 s} \tag{5}$$

$$\tau_c = 0.72 d^{-0.33} \left(\frac{24}{f_{c0}} \right)^{-1/3} \left(\frac{0.012}{p_l} \right)^{-1/3} \tag{6}$$

in which F_{sc} and F_{ss} : shear capacity by concrete and ties (MN), respectively, τ_c : averaged concrete shear strength (MPa), b and d : width and length of the concrete section (m), c_c : modification factor depending on loading condition, A_h and σ_{sy} : sectional area (m^2) and the yield strength of a tie (MPa), f_{c0} : design strength of concrete (MPa), p_l : longitudinal reinforcement ratio in tension, and s : interval of ties (m). The modification factor in accordance with loading condition c_c is a factor which takes account of the deterioration of concrete shear capacity under repeated cyclic loading; c_c is 1.0 under a static load, while it is 0.6 and 0.8 under Type I ground motion (long-duration middle-field ground motions generated by M8 subduction earthquakes) and Type II ground motion (short-duration near-field ground accelerations with long-period pulses), respectively.

Assuming Eq. (3), the shear stress at the upper cut-off vs. the lateral displacement at the column top relation was evaluated as shown in Fig. 15, in which τ_c is normalized in terms of α_c and α_{pl} defined as

$$\alpha_c = \left(\frac{24}{f_c} \right)^{-1/3} ; \quad \alpha_{pl} = \left(\frac{0.012}{p_l} \right)^{-1/3} \tag{7}$$

In Fig. 15, shear stress evaluated for two 1.68m

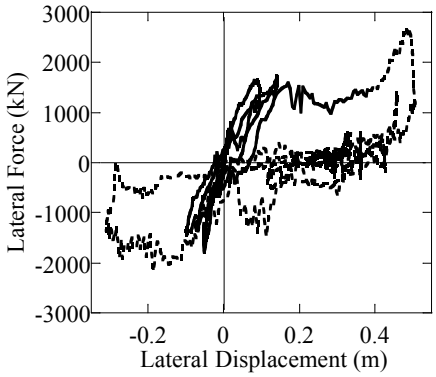

Fig. 14 Lateral force at upper cut-off vs. lateral displacement at the column top hysteresis in the principle response direction

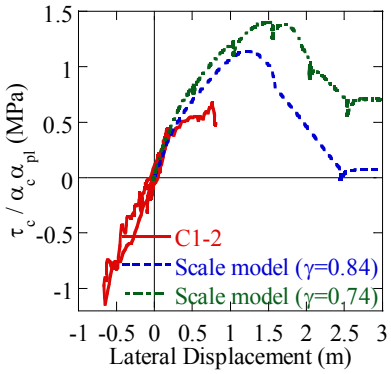

Fig. 15 Shear stress of concrete

tall 400mm diameter scaled model columns with different shear vs. flexure strength ratio is included for comparison [5]. It is seen in Fig. 15 that $\tau_c / \alpha_c \alpha_{pl}$ of C1-2 is 0.68 MPa which is 15 % larger than the value (0.59 MPa) evaluated by Eq. (3).

5. ANALYTICAL CORRELATION FOR C1-5

5.1 Analytical Idealization

The column was idealized by a 3D discrete analytical model including P-Δ effect as shown in Fig. 16. The column was idealized by fiber elements. A section was divided into 400 fibers.

The stress vs. strain constitutive model of confined concrete is assumed as [6]

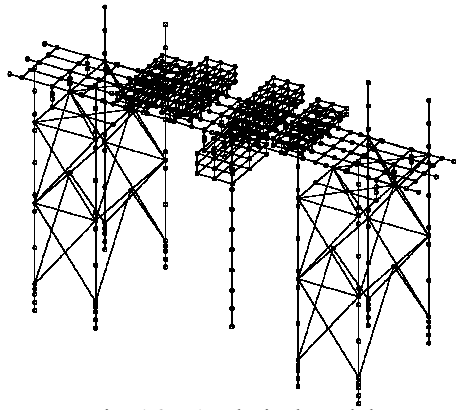

Fig. 16 Analytical model

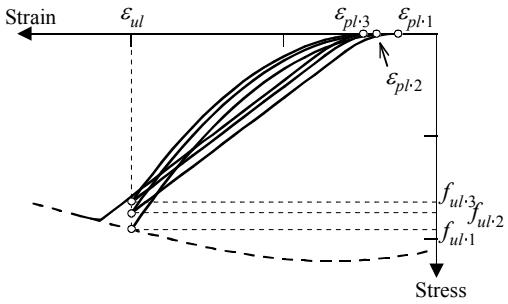

Fig. 17 Unloading and reloading paths of confined concrete

$$f_c = \begin{cases} E_c\varepsilon_c\left\{1-\dfrac{1}{n}\left(\dfrac{\varepsilon_c}{\varepsilon_{cc}}\right)^{n-1}\right\} & (0 \le \varepsilon_c \le \varepsilon_{cc}) \\ f_{cc} - E_{des}(\varepsilon_c - \varepsilon_{cc}) & (\varepsilon_{cc} \le \varepsilon_c \le \varepsilon_{c0}) \\ a\, f_{cc} & (\varepsilon_{c0} \le \varepsilon_c) \end{cases} \tag{8}$$

in which f_{cc} and ε_{cc} = strength of confined concrete and strain corresponding to f_{cc}, E_c = elastic modulus of concrete, E_{des} = gradient at descending branch, a = residual strength factor depending on the confinement, and $n = E_c\varepsilon_{cc}/(E_c\varepsilon_{cc} - f_{cc})$. In Eq. (8), f_{cc}, ε_{cc}, E_{des}, ε_{c0} and a are defined as

$$f_{cc} = f_{c0} + 3.8\alpha\rho_s f_{sy} \tag{9}$$

$$\varepsilon_{cc} = 0.002 + 0.033\beta\frac{\rho_s f_{sy}}{f_{c0}} \tag{10}$$

$$E_{des} = 11.2\frac{{f_{c0}}^2}{\rho_s \cdot f_{sy}} \tag{11}$$

$$\varepsilon_{c0} = \varepsilon_{cc} + 0.8 f_{cc}/E_{des} \tag{12}$$

$$a = 0.2 \tag{13}$$

in which f_{c0} = design strength of concrete, f_{sy} = yield strength of tie bars, α and β = shape factors (α=1.0 and β=1.0 for circular piers), and ρ_s = volumetric ratio of tie bars. Stress vs. strain relation of covering concrete was evaluated by Eq. (3) assuming ρ_s = 0 in Eqs. (9) and (10). E_{des}, ε_{c0} and a are given as

$$E_{des} = \frac{f_{c0}}{\varepsilon_{c0} - \varepsilon_{cc}} \tag{14}$$

$$\varepsilon_{c0} = 0.005 \tag{15}$$

$$a = 0 \tag{16}$$

Unloading and reloading hystereses consist of combinations of full unloading, partial unloading, full reloading and partial reloading. For example, as shown in Fig. 17**,** unloading from an envelop curve and reloading from zero stress are idealized as [7]

$$f_c = f_{ul\cdot1}\left(\frac{\varepsilon_c - \varepsilon_{pl\cdot1}}{\varepsilon_{ul} - \varepsilon_{pl\cdot1}}\right)^2 \tag{17}$$

$$f_c = \begin{cases} 2.5 f_{ul\cdot n}\left(\dfrac{\varepsilon_c - \varepsilon_{pl\cdot n}}{\varepsilon_{ul} - \varepsilon_{pl\cdot n}}\right)^2 & 0 \le \dfrac{\varepsilon_c - \varepsilon_{pl\cdot n}}{\varepsilon_{ul} - \varepsilon_{pl\cdot n}} < 0.2 \\ E_{c\cdot rl}(\varepsilon_c - \varepsilon_{ul}) + f_{ul\cdot n+1} & 0.2 \le \dfrac{\varepsilon_c - \varepsilon_{pl\cdot n}}{\varepsilon_{ul} - \varepsilon_{pl\cdot n}} \le \dfrac{\varepsilon_{re} - \varepsilon_{pl\cdot n}}{\varepsilon_{ul} - \varepsilon_{pl\cdot n}} \end{cases} \tag{18}$$

where

$$\varepsilon_{pl\cdot1} = \begin{cases} 0 & 0 \le \varepsilon_{ul} \le 0.001 \\ 0.43(\varepsilon_{ul} - 0.001) & 0.001 < \varepsilon_{ul} < 0.0035 \\ 0.94(\varepsilon_{ul} - 0.00235) & \varepsilon_{ul} \ge 0.0035 \end{cases} \tag{19}$$

in which $f_{ul\cdot1}$ and ε_{ul} = unloading stress and strain on the envelope curve, $f_{ul\cdot n}$ = stress at the unloading point after n th unloading/reloading, $\varepsilon_{pl\cdot n}$ = plastic strain after n th unloading & reloading, ε_{re} = strain at the point where reloading path intersects the envelope curve, and $E_{c\cdot rl}$ = reloading modulus.

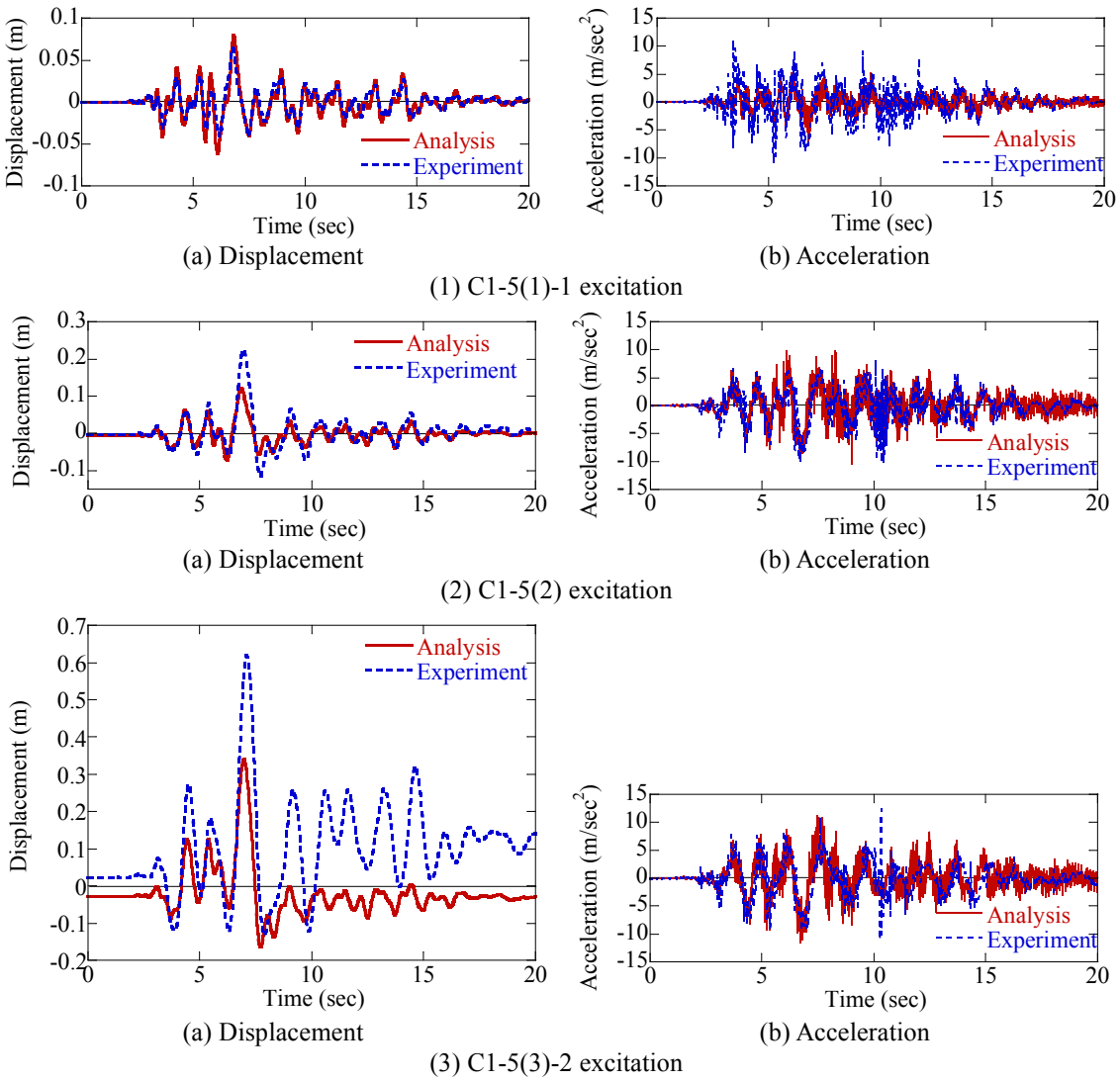

Fig. 18 Analytical correlation for the response displacements and accelerations at the column top in the principle response direction

Modified Menegotto-Pinto model was used to idealize the stress vs. strain relation of longitudinal bars [8, 9].

5.2 Analytical Correlation

Fig. 18 shows the analytical correlation on the response displacements at the top of the column in the principal direction during C1-5(1)-1, C1-5(2) and C1-5(3)-2 excitations. Fig. 19 compares the measured and computed moment at the base vs. lateral displacement at the column top hysteresis during the three excitations. Because nonlinear hysteretic response was still limited during C1-5(1)-1 excitation, the computed response displacement and moment vs. lateral displacement hysteresis are quite in good agreement with the experimental results, however as C1-5 suffered more damage, the accuracy of analytical prediction decreases.

Consequently, it is required to develop an analytical model that can predict the response of the columns until collapse for realizing reliable performance based seismic design.

6. COCLUSIONS

A preliminary result on a series of shake table experiment and analysis to three full-size reinforced concrete columns was presented. Based

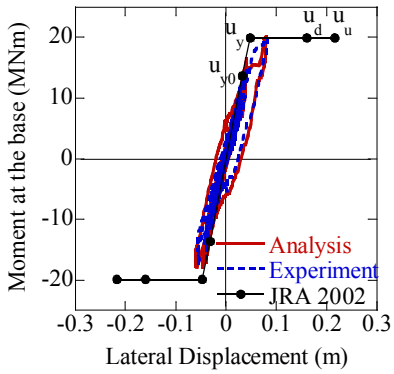

(a) C1-5(1)-1 excitation

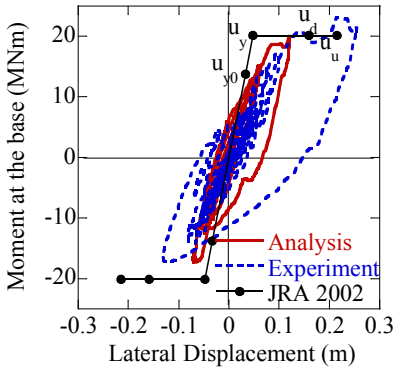

(b) C1-5(2) excitation

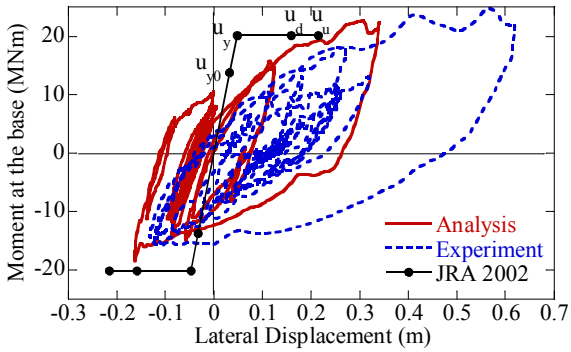

(c) C1-5(3)-2 excitation

Fig. 19 Moment at the base vs. lateral displacement at the column top hysteresis in principle response direction

on the results presented herein, the following tentative conclusions may be deduced;

1) C1-1 which is a typical column in the 1970s suffered extensive damage under C1-1-1 excitation. The progress of damage during C1-1-2 excitation was extensive even though it was anticipated before the experiment that damage would not progress unless the intensity of second excitation was much larger than that of the first excitation. This resulted from the extensive deterioration of the lateral confinement due to separation of ties at the lap splices. It is highly possible that columns without sufficient lateral confinement have a similar progress of damage during a long-duration near-field ground motion or strong aftershocks.

2) C1-5 which is a typical column in accordance with the current design criteria suffered only a few numbers of horizontal cracks with the maximum width of 1 mm under C1-5 (1)-1 excitation. The ultimate drift was 2.9 % which was 2.2 times larger than that of C1-1. Consequently, enhancement of the seismic performance of C1-5 compared to C1-1 is obvious. However the progress of failure of C1-5 was extensive when it was subjected to 25 % stronger excitation under 21% added mass (C1-5(3) excitations). Blocks of crashed core concrete spilled out like explosion from the steel cages. The seismic performance of C1-5 subjected to longer duration near-field ground motion has to be carefully evaluated.

3) C1-2 failed in shear at the upper cut-off. As soon as circular ties at the upper cut-off yielded, a small diagonal cracks developed. As they extended to several major diagonal cracks, C1-2 completely failed in shear within less than 2.5 s since the initiation of a couple of small diagonal cracks. Concrete blocks crashed by shear and deformed longitudinal bars extensively moved out from the inside of column.

4) The lateral confinement in the flexure dominant columns is not uniform around the ties as it is currently assumed in design. More importantly, the lateral confinement of multi layered ties is very complex. Strains of ties are not similar among the multi-layered ties, and they are related to the degree of constraint exerted for preventing local buckling of longitudinal bars. Strains are generally larger in the outer ties than the inner ties. This implies that the lateral confinement by Eq. (2) can be overestimated.

5) Computed response for the flexure dominant columns is satisfactory while response undergoes the moderate nonlinear range, however accuracy of the analytical prediction deteriorates once the columns undergo the strong nonlinear range. An analytical model which can predict response of the columns until failure should be developed for enhancing the reliability of the performance based seismic design.

ACKNOWLEDGEMENTS

The C1 experiment was conducted based on the extensive support of over 70 personnel in the Overview Committee (Chair, Professor Emeritus Hirokazu Iemura, Kyoto University), Executing Committee of Large-scale Bridge Experimental Program (Chair, Professor Kazuhiko Kawashima, Tokyo Institute of Technology), Analytical Correlation WG (Chair, Dr. Shigeki Unjoh, Public Works Research Institute), Measurements WG (Chair, Professor Yoshikazu Takahashi, Kyoto University), Dampers & Bearings WG (Chair, Dr. Masaaki Yabe, Chodai) and Blind Analysis WG (Chair, Professor Hiroshi Mutsuyoshi, Saitama University). Their strong support is greatly appreciated. Invaluable support and encouragement of Professor Stephen Mahin, University of California, Berkeley and Professor Ian Buckle, University of Nevada, Reno are greatly appreciated.

REFERENCES

1. Nakashima, M., Kawashima, K., Ukon, H. and Kajiwara, K.: Shake table experimental project on the seismic performance of bridges using E-Defense, S17-02-010 (CD-ROM), 14 WCEE, Beijing, China, 2008.
2. Kawashima, K. Sasaki, T., Kajiwara, K., Ukon, H., Unjoh, S., Sakai, J., Takahashi, Y., Kosa, K., and Yabe, M.: Seismic performance of a flexural failure type reinforced concrete bridge column based on E-Defense excitation, Proc. JSCE, A, Invited paper, 1-19, JSCE, 2009 (in print).
3. Kawashima, K. and Unjoh, S.: The damage of highway bridges in the 1995 Hyogo-ken nanbu earthquake and its impact on Japanese seismic design, Journal of Earthquake Engineering, 1(3), 505-542, 1997.
4. Kono, H., Watanabe, H. and Kikumori, Y.: Shear strength of large RC beams, Technical Note, 3426, Public Works Research Institute, Tsukuba, Japan, 1996.
5. Sasaki, T., Kurita, H. and Kawashima,K.: Seismic performance of RC bridge columns with termination of main reinforcement with inadaquate development, S17-02-009 (CD-ROM), 14WCEE, Beijing, China, 2008.
6. Hoshikuma, J., Kawashima, K., Nagaya, K. and Taylor, A.W.: Stress-strain model for confined reinforced concrete in bridge piers, Journal of Structural Engineering, ASCE, 123(5), 624-633, 1997.
7. Sakai, J. and Kawashima, K.: Unloading and reloading stress-strain model for confined concrete, Journal of Structural Engineering, ASCE, 132 (1), 112-122, 2006.
8. Menegotto, M. and Pinto, P.E.: Method of analysis for cyclically loaded R.C. plane frames including changes in geometry and non-elastic behavior of elements under combined normalized force and bending, Proc. IABSE Symposium on Resistance and Ultimate Deformability of Structures Acted on by Well Defined Repeated Loadings, 15-22, 1973.
9. Sakai, J. and Kawashima, K.: Modification of the Giuffre, Menegotto and Pinto model for unloading and reloading paths with small strain variations, Journal of Structural Mechanics and Earthquake Engineering, JSCE, 738/I-64, 159-169. 2003.
10. Priestley, M.N.J., Seible, F. and Calvi, G.M.: Seismic design and retrofit of bridges, John Wiley & Sons, New York, USA, 1996.